doi:10.1093/brain/aws110 Brain 2012: 135; 1736–1750 | 1736

BRAIN
A JOURNAL OF NEUROLOGY

Microangiopathy in the cerebellum of patients with mitochondrial DNA disease

Nichola Z. Lax,[1,2] Ilse S. Pienaar,[1,2] Amy K. Reeve,[1,2] Philippa D. Hepplewhite,[1] Evelyn Jaros,[3,4,5] Robert W. Taylor,[1] Raj N. Kalaria[2] and Doug M. Turnbull[1,2]

1 The Wellcome Trust Centre for Mitochondrial Research, Institute for Ageing and Health, Newcastle University, Newcastle upon Tyne, NE2 4HH, UK
2 Newcastle University Centre for Brain Ageing and Vitality, Institute for Ageing and Health, Newcastle University, Framlington Place, Newcastle upon Tyne, NE2 4HH, UK
3 Neuropathology/Cellular Pathology, Royal Victoria Infirmary, Queen Victoria Road, Newcastle upon Tyne, NE1 4LP, UK
4 Institute for Ageing and Health, Newcastle University, Campus for Ageing and Vitality, Newcastle upon Tyne, NE4 5PL, UK
5 UK NIHR Biomedical Research Centre for Ageing and Age-related disease award to the Newcastle upon Tyne Hospitals NHS Foundation Trust, UK

Correspondence to: Prof. D.M. Turnbull,
The Wellcome Trust Centre for Mitochondrial Research,
Institute for Ageing and Health,
Newcastle University,
Newcastle upon Tyne, NE2 4HH, UK
E-mail: doug.turnbull@newcastle.ac.uk

Neuropathological findings in mitochondrial DNA disease vary and are often dependent on the type of mitochondrial DNA defect. Many reports document neuronal cell loss, demyelination, gliosis and necrotic lesions in post-mortem material. However, previous studies highlight vascular abnormalities in patients harbouring mitochondrial DNA defects, particularly in those with the m.3243A>G mutation in whom stroke-like events are part of the mitochondrial encephalopathy lactic acidosis and stroke-like episodes syndrome. We investigated microangiopathic changes in the cerebellum of 16 genetically and clinically well-defined patients. Respiratory chain deficiency, high levels of mutated mitochondrial DNA and increased mitochondrial mass were present within the smooth muscle cells and endothelial cells comprising the vessel wall in patients. These changes were not limited to those harbouring the m.3243A>G mutation frequently associated with mitochondrial encephalopathy, lactic acidosis and stroke-like episodes, but were documented in patients harbouring m.8344A>G and autosomal recessive *polymerase (DNA directed), gamma* (*POLG*) mutations. In 8 of the 16 patients, multiple ischaemic-like lesions occurred in the cerebellar cortex suggestive of vascular smooth muscle cell dysfunction. Indeed, changes in vascular smooth muscle and endothelium distribution and cell size are indicative of vascular cell loss. We found evidence of blood–brain barrier breakdown characterized by plasma protein extravasation following fibrinogen and IgG immunohistochemistry. Reduced immunofluorescence was also observed using markers for endothelial tight junctions providing further evidence in support of blood–brain barrier breakdown. Understanding the structural and functional changes occurring in central nervous system microvessels in patients harbouring mitochondrial DNA defects will provide an important insight into mechanisms of neurodegeneration in mitochondrial DNA disease. Since therapeutic strategies targeting the central nervous system are limited, modulating vascular function presents an exciting opportunity to lessen the burden of disease in these patients.

Keywords: mitochondrial diseases; mitochondrial DNA; microangiopathy; cerebellum; blood–brain barrier

Abbreviations: COX = cytochrome *c* oxidase; MELAS = mitochondrial encephalomyopathy with lactic acidosis and stroke-like episodes; ZO-1 = zona occludin-1

Received December 6, 2011. Revised February 8, 2012. Accepted March 16, 2012. Advance Access publication May 9, 2012

Introduction

Mitochondrial DNA diseases are a clinically heterogeneous group of multisystem disorders, with neurological deficits among the most prominent and disabling features (DiMauro and Schon, 2008). These neurological features typically include cerebellar ataxia, epilepsy, peripheral neuropathy and dementia. Involvement of the mitochondrial genome (mitochondrial DNA), whether due to primary mitochondrial DNA mutations (such as point mutations or complex rearrangements of mitochondrial DNA) or secondary mitochondrial DNA defects, such as depletion or deletions, caused by nuclear mutations, is frequently responsible for the development of mitochondrial disease (Tuppen *et al*., 2010). A number of pathological studies have tried to explain the underlying neuropathology in these patients and these often include features of neuronal cell loss, astrogliosis and white matter changes (Sparaco *et al*., 1993; Tanji *et al*., 1999*a*, *b*).

The presence of cytochrome *c* oxidase (COX)-deficient and/or intensely succinate dehydrogenase reactive vessels containing increased mitochondrial DNA copy number and enlarged mitochondria on electron microscopy have been described in both non-CNS and CNS tissues (Ohama *et al*., 1987, 1988; Hasegawa *et al*., 1991; Tokunaga *et al*., 1993; Love and Hilton, 1996; Betts *et al*., 2006). This increase in COX-deficiency has been attributed to a high mutation load within the smooth muscle cells comprising the CNS vasculature. Typically, these findings have been shown in patients harbouring the common m.3243A > G mutation associated with mitochondrial encephalomyopathy with lactic acidosis and stroke-like episodes (MELAS) where stroke-like episodes are particularly frequent (Betts *et al*., 2006). Additionally, Tanji *et al*. (2001) have shown a decrease in the level of expression of mitochondrially encoded COX subunit II in the CNS microvasculature of patients with MELAS (Tanji *et al*., 2001).

The pathological consequences of the neurovascular COX-deficiency are not well understood. Stroke-like episodes are thought to contribute to the genesis of ischaemic-like lesions, which typically manifest focally in the posterior cortical regions of the brain (Sue *et al*., 1998). They resemble true infarcts in that they are pan-necrotic and demonstrate profound neuronal cell loss, microvacuolation, gliosis and eosinophilia in surviving neurons but their topographical distribution does not follow the vascular territories of major cerebral arteries or border zones. Although stroke-like episodes are part of the clinical syndrome in MELAS (Pavlakis *et al*., 1984), more recently stroke-like episodes have been documented in patients harbouring the m.8344A > G mutation associated with myoclonic epilepsy ragged red fibres and autosomal recessive mutations in the *POLG* gene encoding for catalytic subunit of the polymerase gamma protein, which is responsible for mitochondrial DNA replication (Tanji *et al*., 2003; Deschauer *et al*., 2007). Regions of necrotic cortical lesions without clinical manifestation of stroke-like episodes has also been seen in *POLG* mutations typically confined to the posterior occipital lobe regions (Winterthun *et al*., 2005; Tzoulis *et al*., 2006, 2010).

Although the genesis of ischaemic-like lesions in mitochondrial DNA disease is not well understood, a number of suggestions have been proposed. These include the presence of dysfunctional mitochondria within the vessel wall, which might be causal for infarct formation (Ohama *et al*., 1987; Hasegawa *et al*., 1991) with treatment with L-arginine decreasing both the frequency and severity of stroke-like episodes in MELAS (Koga *et al*., 2005, 2010). Alternatively, energy failure within the neurons and glial cells is primarily responsible for ischaemic-like lesions (Gilchrist *et al*., 1996; Betts *et al*., 2006). Finally, neuronal hyperexcitability may act as a trigger for the initiation of stroke-like episodes and therefore formation of lesions (Iizuka *et al*., 2002, 2003, 2007; Iizuka and Sakai, 2005).

The principle aim of this study was to determine the extent of vascular abnormalities in patients harbouring mitochondrial DNA defects in the cerebellum, a region of the brain frequently involved in patients with mitochondrial DNA disease. Previously, we have shown that ataxia is a common symptom in patients with mitochondrial DNA disease and results from degeneration of the cerebellum (Lax *et al*., 2012*a*). The current study aimed to determine whether the abnormalities of vasculature morphology and evidence of respiratory chain deficiency correlated with the presence of ischaemic-like lesions. In addition, we wanted to determine which microvascular components demonstrated biochemical defects and whether this correlated with the genetic defect. We were able to show not only that the respiratory chain dysfunction in smooth muscle and endothelial cells was associated with presence of ischaemic-like lesions but also, with breakdown of the blood–brain barrier in areas not affected by lesions. Targeting the blood vessel abnormalities may provide an important therapeutic approach for many patients with mitochondrial DNA disease.

Materials and methods

Clinical details and neurohistopathology

The patients included in this study consisted of 16 subjects with a variety of primary or secondary mitochondrial DNA defects and five age-matched, neurologically normal controls (Table 1). All control cases were matched to patients for age, gender, post-mortem interval and length of tissue fixation. Local research ethical approval and full consent for brain tissue retention and research was obtained and the CNS tissues were processed by the Newcastle Brain Tissue Resource (NBTR). Tissue processing and general neurohistopathological staining was performed as previously described (Betts *et al*., 2006).

Immunohistochemistry using chromogens

A range of primary antibodies (Supplementary Table 1) were used to evaluate protein components comprising the mitochondrial respiratory chain; including porin, complex I 20 kDa, complex II 70 kDa and complex IV subunit I, vasculature markers; including smooth muscle cells, endothelial cells, astrocytes and collagen IV and finally plasma proteins; including fibrinogen and IgG (detailed in Supplementary Table 1). Serial sections of formalin-fixed paraffin-embedded sagittal cerebellum were cut at 5 μm using a microtome (Microm International)

Table 1 Characteristics of patients

	Pt 1	Pt 2	Pt 3	Pt 4	Pt 5	Pt 6	Pt 7	Pt 8	Pt 9	Pt 10	Pt 11	Pt 12	Pt 13	Pt 14	Pt 15	Pt 16
Age at death	60	57	45	36	42	20	30	45	42	58	34	55	40	24	59	50
Gender	F	F	M	F	F	F	M	M	F	M	F	M	F	F	M	M
Genotype	m.3243A>G	m.3243A>G	m.3243A>G	m.3243A>G	m.3243A>G	m.3243A>G	m.3243A>G	m.3243A>G	m.8344A>G	m.8344A>G	m.13094T>C	m.14709T>C	Single, large-scale mtDNA deletion	*POLG* (p.Ala467Thr, p.Trp748Ser) and multiple mtDNA deletions	*POLG* (p.Gly848Ser, p.Ser1104Cys) and multiple mtDNA deletions	POLG (p.Ala467Thr, p.X1240Cys)- and multiple mtDNA deletions
Disease duration (years)	33	32	8	15	22	10	11	15	37	20	2	21	37	4	37	35
Clinical diagnosis	MELAS, depression, encephalopathy, myopathy, constipation	MELAS, depression, cardiomyopathy, irritable bowel	MELAS, dementia, encephalopathy, constipation.	MELAS, dementia, encephalopathy, optic atrophy	MELAS, myoclonus, myopathy, depression	MELAS, dementia, encephalopathy, deafness, irritable bowel	Cardiomyopathy, peripheral neuropathy, myopathy, opthalmoplegia	MELAS, epilepsy	MERRF, myopathy, myoclonus, depression	MERRF, myopathy, myoclonus	MELAS/Leigh disease, myoclonus, fatigue	Dementia, peripheral neuropathy, diabetes, opthalmoplegia	KSS, encephalopathy, depression.	Encephalopathy, dementia, peripheral neuropathy, depression	Opthalmoplegia, dementia, peripheral neuropathy, depression.	Sensory neuropathy, encephalopathy, dementia.
Ataxia	+	+	+	+	+	+	+	+	+	+	+	+	+	+	+	+
Migraine	+		+								+					
Stroke-like episodes	+	+	+	+	+	+		+			+					
Seizures	+		+	+				+	+	+	+			+		+
Previously published	(Lax *et al.*, 2012*a*)	(Lax *et al.*, 2012*a*)	(Lax *et al.*, 2012*a*)	(Lax *et al.*, 2012*a*)	(Lax *et al.*, 2012*a*)	(Lax *et al.*, 2012*a*)	(Lax *et al.*, 2012*a*)		(Lax *et al.*, 2012*a*)		(Lax *et al.*, 2012*a*)	(Lax *et al.*, 2012*a*)	(Lax *et al.*, 2012*a*, *b*)	(Lax *et al.*, 2012*a*, *b*)	(Betts-Henderson *et al.*, 2009; Lax *et al.*, 2012*a*, *b*)	(Lax *et al.*, 2012*a*, *b*)

F = female; KSS = Kearns–Sayre syndrome; M = male; MERRF = myoclonic epilepsy with ragged red fibres; Pt = Patient; + denotes the presence of symptom.

and mounted on to SuperFrost™ slides (Thermo Fisher Scientific). Immunohistochemical staining was performed as previously described using a polymer detection system (Menarini Diagnostics) (Lax *et al*., 2012*b*). Vascular markers for vascular smooth muscle cells, endothelial cells and collagen IV were optimized using the avidin-biotin complex (ABC) detection method. Briefly, this involved deparaffinization and rehydration of the tissue sections followed by antigen retrieval according to the primary antibody used (Supplementary Table 1). Sections were washed well in distilled water and incubated in 3% hydrogen peroxide solution (Sigma) for 30 min to block endogenous peroxidases. The sections were then washed in Tris-buffered saline pH 7.4 and blocked in 1% normal goat serum. The required primary antibody was then applied at the appropriate dilution (Supplementary Table 1) at room temperature for 90 min. Following a Tris-buffered saline pH 7.4 wash, biotinylated anti-mouse or anti-rabbit secondary antibodies diluted 1:200 (Vector Laboratories) were then incubated with the sections for 30 min. This was followed by a Tris-buffered saline pH 7.4 wash and application of the VECTASTAIN® Elite ABC (Vector Laboratories) for 30 min. The sections were washed well in distilled water before application of 3,3′-diaminobenzadine (DAB; Sigma) for 5 min and a haematoxylin counterstain to allow visualization of the marker of interest.

Quantitative measurement of alpha-smooth muscle actin and collagen IV immunoreactivity within arterioles

Quantitative measurements of collagen IV- and alpha-smooth muscle actin-positive layers within the microvasculature were obtained from controls ($n = 4$) and patients harbouring m.3243A > G ($n = 4$). Sections (5-μm thick) stained for collagen IV or alpha-smooth muscle actin were viewed on an Olympus microscope (Olympus BX54) under a low magnification. The white matter of the cerebellum was outlined using StereoInvestigator (MBF Bioscience) and a meander scan was initiated throughout this region at ×10 magnification. All arterioles with a diameter >50 μm were quantified by measuring the internal and external diameter of the vessel wall which was immune-positive for collagen IV or alpha-smooth muscle actin (modified from Yamamoto *et al*., 2009). These measurements were performed three times per vessel. The thickness of the alpha-smooth muscle actin- or collagen IV immunopositive layer was then derived by the following equation: layer thickness = (external diameter − internal diameter)/2. A total of 86 and 134 collagen IV-positive and 77 and 192 alpha-smooth muscle actin-positive vessels were analysed in control and m.3243A > G tissues, respectively. As the data were not normally distributed, statistical significance was assessed using GraphPad Prism® software (version 5, GraphPad Inc., http://www.graphpad.com/prism/) using Kruskal Wallis with *post hoc* analysis performed using Dunn's multiple comparison test. Statistical significance was determined when $P < 0.05$.

Immunofluorescence for identification of tight junctions

Dual immunofluorescence was utilized to detect the endothelial cell layer and tight junction proteins, zona occludin-1 (ZO-1) and occludin in control ($n = 5$), and patients with m.3243A > G ($n = 4$) and m.8344A > G ($n = 1$). Patients were selected on the basis of the COX-deficiency and pathological changes in the microvasculature. Three 6 μm formalin-fixed paraffin-embedded sections were cut at equally spaced intervals of a minimum of 25 μm to enable random sampling. These sections were deparaffinized and rehydrated as described above. Heat-mediated antigen retrieval was performed by microwaving sections in citrate buffer (pH 6). Sections were washed well in distilled water and incubated with 3% normal goat serum (Sigma) for 30 min. The primary antibodies anti-GLUT1 and anti-ZO-1 and anti-GLUT1 and anti-occludin were then applied at the optimal dilution in 0.1% Triton-X and 1% normal oat serum Tris-buffered saline solution (Supplementary Table 2) overnight at 4°C. The following day, sections were washed three times for 5 min with Tris-buffered saline and incubated with the appropriate secondary antibodies (Supplementary Table 2) for 1 h at 37°C. This was followed by three 5-min washes with Tris-buffered saline. To amplify the signal of tight junction primary antibodies, a biotinylated secondary antibody was used and sections were incubated with Rhodamine-Red-X-Streptavidin for 1 h at 37°C (Supplementary Table 2). Finally, to minimize autofluorescence the sections were incubated in 0.5% Sudan black in 70% ethanol for 5 min and rinsed in running tap water for 3 min. Sections were coverslipped in hard-set mounting medium (Vector Laboratories) and allowed to dry overnight at 4°C.

Analysis of immunofluorescence

Images of the dual fluorescently-stained sections were acquired using a spinning disc confocal laser-scanning microscope (Zeiss) mounted on an axio observer (C1, Zeiss) and equipped with AxioVision imaging software (v.4.8). The images were captured at high magnification using a ×63/1.30 numerical aperture objective lens and a Photometrix QuantEM™ 512SC camera. *Z*-stacked imaging (three different levels, every 1.5 μm) was carried out across the length, breadth and depth of each specimen. Photographs were taken at these levels with identical exposure times (400 ms), gain and offsets used for each image acquisition across conditions. Moreover, fluorescent images were always taken under identical conditions for laser excitation (488 for FITC Alexa 488 green and 561 for rhodamine red) and emission (527/55 nm and 645/60 nm, respectively). Six random regions of interest were identified per section.

Automated maximum intensity projection 16-bit (508 × 508 pixels) file images were generated for each channel and imported into ImageJ software (NIH). Blinded analysis was performed on the digital images by tracing the outline of vessels manually. The integrated optical density for individual vessels was calculated to represent the intensity of fluorescence for antibodies targeting GLUT-1, ZO-1 and occludin per unit area outlined, in accordance with previously published protocols (Fuseler *et al*., 2006, 2010; Guan *et al*., 2011).

All results were statistically analysed using GraphPad Prism® software (version 5, GraphPad Inc., http://www.graphpad.com/prism/). The raw data values (given as fluorescent intensity) for all three proteins (GLUT1, ZO-1, occludin) failed a D'Agostino and Pearson omnibus normality test; thus data were analysed using non-parametric tests. We tested for significant differences between control groups versus patients with m.3243A > G using a Kruskall–Wallis test followed by a Dunn's Multiple Comparison test. Analysis of the fluorescence intensity values for ZO-1 and occludin positive vessels between control versus m.3243A > G vessels was performed using a Mann–Whitney U-test. The results for the fluorescence intensity analysis are given as the means ± standard deviation (SD).

Dual cytochrome c oxidase/succinate dehydrogenase histochemistry

A dual histochemical assay for COX and succinate dehydrogenase activities was used to identify COX-deficient/succinate

dehydrogenase-positive cells within the vasculature. This was performed on frozen 10 μm cerebellum sections as previously described (Betts *et al*., 2006).

Isolation of mitochondrial DNA from smooth muscle cells

Vascular smooth muscle cells were visualized using an immunostaining method designed to identify alpha-smooth muscle actin on frozen sections (20 μm) mounted on polyethylene naphthalate-membrane slides (Leica). Firstly, fixation of the tissue was performed in cold acetone for 10 min followed by incubation in 3% hydrogen peroxide for 20 min and incubation in 1% normal goat serum for 30 min. Following this, sections were incubated with a mouse anti-alpha smooth muscle actin (Dako) diluted 1:1000 for 1 h, followed by three 5-min washes with Tris-buffered saline and incubation in biotinylated-secondary antibody (goat anti-mouse IgG; Vector Laboratories) diluted 1:200 for 30 min. This was followed by three 5-min washes in Tris-buffered saline and incubated in a VECTASTAIN® Elite ABC solution (Vector Laboratories) and visualized with 3,3′-diaminobenzidene (Sigma). Sections were dehydrated through ethanol (Alanar) series and stored at −20°C. Isolation of the smooth muscle cell wall was performed using laser microcapture dissection (Leica Microsystems LMD6000). Vascular smooth muscle cell layers were selected based on staining and morphology. Following capture, cells were lysed with a standard lysis buffer overnight (Taylor *et al*., 2003).

Isolation of mitochondrial DNA from endothelial cells

The endothelium was visualized using a similar immunostaining protocol for identification of smooth muscle cells. The main differences included frozen sections (15 μm) mounted on glass slides, the primary antibody consisted of rabbit anti-GLUT1 (Fisher Scientific) diluted 1:300 and the secondary antibody consisted of a biotinylated goat anti-rabbit IgG diluted 1:200 (Vector Laboratories). Antibody signal was developed using the ABC kit and finally visualized with 3,3′-diaminobenzidene (Sigma). Sections were dehydrated through an ethanol (Alanar) series and stored in a 50% ethanol (Alanar) solution at 4°C. Isolation of the endothelial cell layer was performed using a light microscope with an attached micromanipulator (Leica). Vessel layers were selected based on staining and morphology. Following capture, cells were lysed with a standard lysis buffer overnight (Taylor *et al*., 2003).

Pyrosequencing to determine percentage heteroplasmy level of mutated mitochondrial DNA

The quantitation of mutated mitochondrial DNA heteroplasmy levels for point mutations including m.3243A>G, m.8344A>G and m.13094T>C was performed using PyroMark™ Q24 platform (Qiagen) as previously described (Alston *et al*., 2010; Lax *et al*., 2012*a*).

Quantitative real-time polymerase chain reaction

A multiplex real-time PCR *MT-ND1/MT-ND4* assay was used to quantify the levels of mitochondrial DNA deletions in isolated vessels according to previously described methods (Bender *et al*., 2006; Krishnan *et al*., 2007).

Results

Neurohistopathology of the microvasculature

In the current study, 8 out of 16 patients demonstrated evidence of multiple, pan-necrotic lesions in the posterior inferior cerebellar cortex characterized by tissue destruction as well as neuronal cell loss. Typically, lesions occurred in patients harbouring the m.3243A>G (6/7 patients) and m.8344A>G (1/1 patient) point mutations and autosomal recessive p.Ala467Thr and p.Trp748Ser *POLG* mutations (1/1 patient) (Table 2). This is exemplified by Fig. 1 where a control cerebellar cortex is shown (Fig. 1A) relative to patient with m.3243A>G cerebellar cortex (Fig. 1B) affected by a ischaemic-like lesion involving the molecular, Purkinje cell and granular cell layers. In addition, microvascular mineralization was observed in two patients with m.3243A>G, predominantly in the arterioles within the deep white matter of the cerebellum (Fig. 1C and D). No morphological changes to the white matter myelin components were detected around the affected microvasculature.

Table 2 Summary of the vascular abnormalities occurring in the cerebellum of patients with mitochondrial DNA defects

	Pt 1	Pt 2	Pt 3	Pt 4	Pt 5	Pt 6	Pt 7	Pt 8	Pt 9	Pt 10	Pt 11	Pt 12	Pt 13	Pt 14	Pt 15	Pt 16
Frozen tissue available for analysis	+	−	−	+	−	+	+	+	+	+	+	+	+	+	+	+
Evidence of vascular COX-deficiency	+	ND	ND	+	ND	+	+	+	+	+	−	−	−	ND	−	−
Fixed tissue available for analysis	+	+	+	+	+	+	+	−	+	−	+	+	+	−	+	−
Presence of microinfarct	+	+	+	+	−	+	+	−	−	−	−	−	−	−	−	−
Presence of vessel mineralisation	−	−	−	−	−	+	+	−	−	−	−	−	−	−	−	−
Deposition of collagen IV	↑	↔	↔	↑	↔	ND	*↑	ND	↑	ND	↑	↔	ND	ND	ND	ND
Mitochondrial density in vasculature	↑	↑	↑	↑	↑	↓	ND	ND	↑	ND	↑	↑	↑	↓	↔	↑
Extravascular plasma proteins	ND	+	−	+	+	+	+	+	ND	ND	ND	ND	−	−	+	ND
Neuronal/glial uptake of plasma proteins	ND	+	−	+	+	−	+	−	ND	ND	ND	ND	+	−	+	ND
Purkinje cells immunoreactivity (%)	ND	1	0	60–70	50	0	30	0	ND	ND	ND	ND	20	0	50	ND

+ = present; − = absent; ↑ = increased; ↓ = - decreased; ↔ = no change; ND = not determined (due to lack of tissue); Pt = Patient.

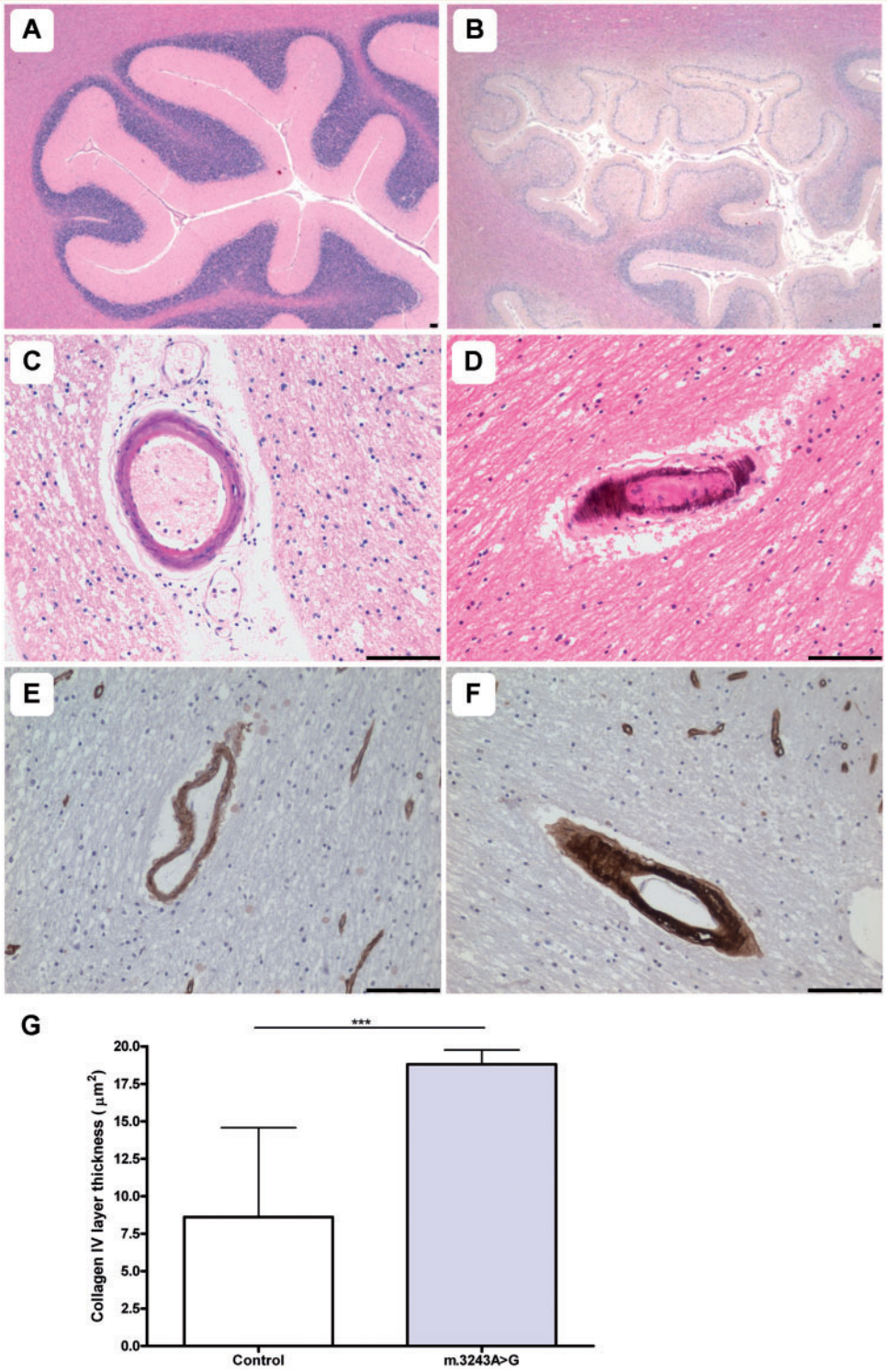

Figure 1 Pathological changes in small vessel morphology are observed in the cerebellum. Relative to control (**A**; haematoxylin and eosin), the cerebellar cortex of a patient harbouring m.3243A>G shows evidence of an ischaemic-like lesion involving the molecular, Purkinje cell and granular cell layers and the underlying white matter (**B**; Patient 6; haematoxylin and eosin). Arteriole mineralization is prominent in patients harbouring the m.3243A>G mutation (**C** and **D**; Patients 6 and 7; haematoxylin and eosin). Relative to control vessels (**E**; collagen IV), numerous patient vessels show increased deposition of collagen IV (**F**; Patient 7; collagen IV). Quantitation of the collagen IV immunopositive layer reveals a significant increase in collagen IV within the basement membrane of arterioles from patients with the m.3243A>G mutation relative to control vessels (**G**; $***P < 0.0001$). Scale bars = 100 μm.

Collagen IV immunostaining

We also documented changes in the pattern of collagen IV staining in those patients demonstrating vascular COX-deficiency (Table 2). Typically an increase in collagen IV deposition in the basement membrane was observed (Fig. 1E and F). Indeed quantitation of the thickness of the collagen IV immunopositive layer within arterioles demonstrated a significant increase in patients harbouring the m.3243A>G mutation relative to controls (Fig. 1G; $P < 0.0001$).

Mitochondrial dysfunction in the microvasculature

All controls used in this analysis demonstrated normal COX activity (Fig. 2A). However, widespread vascular COX-deficiency was detected in patients harbouring the m.3243A>G (Fig. 2B; $n = 4$) and m.8344A>G (Fig. 2C; $n = 2$) point mutations. This was most prominent in the white matter arterioles, where COX-deficiency was present in both the vascular smooth muscle cell and endothelial cell layers, but was also detected in the meninge vessels (Fig. 2B). Interestingly, two patients (Patients 4 and 7) demonstrated striking COX-deficiency in the endothelial cells of capillaries throughout the dentate nucleus, while the dentate neuronal cell populations revealed intact COX activity (Fig. 2D). COX activity was normal in the microvasculature of control cases and patients harbouring the m.13094T>C mutation (Patient 11), a single large-scale mitochondrial DNA deletion (Patient 14) and recessive *POLG* mutations (Patients 16 and 17). Unfortunately due to unavailability of frozen tissue, some patients could not be assessed for COX activity (e.g.

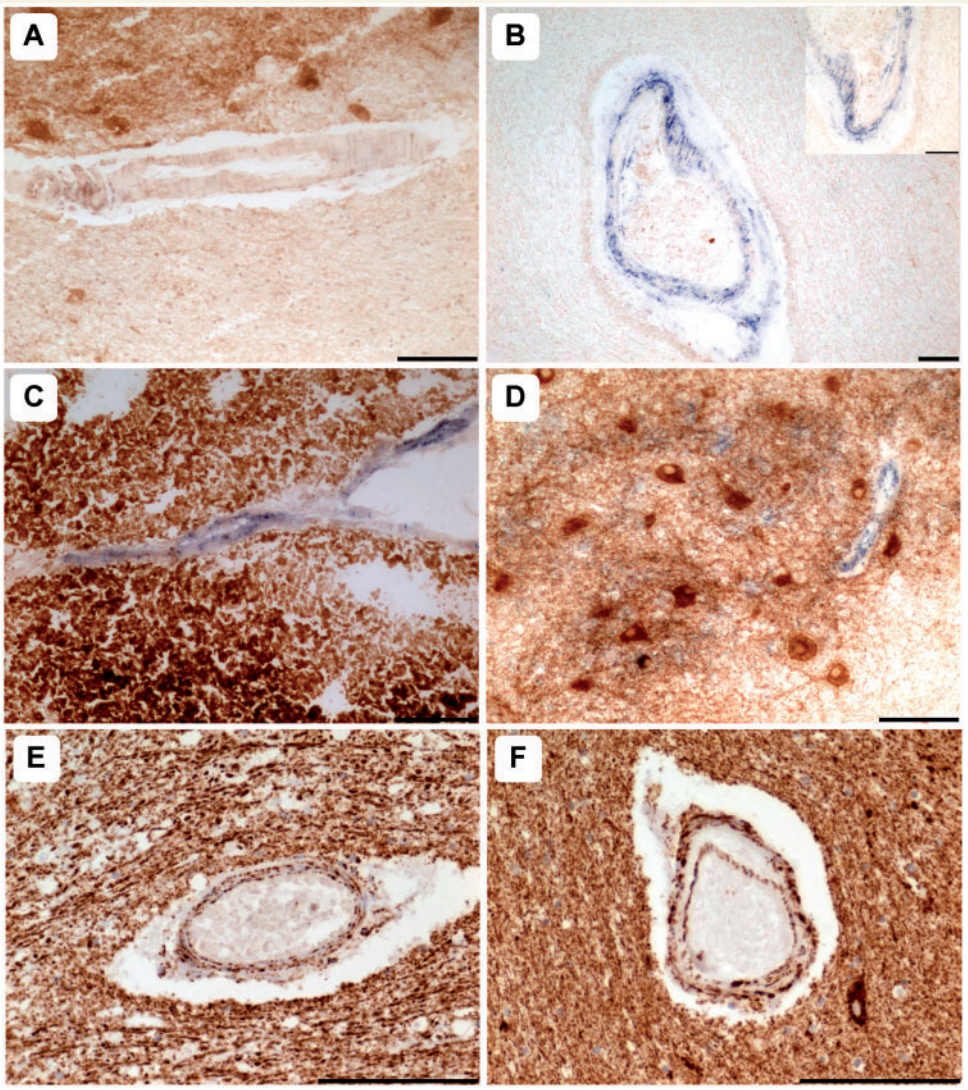

Figure 2 Mitochondrial dysfunction is prominent in patients harbouring m.3243A>G and m.8344A>G point mutations. Relative to control vessels (**A**), COX-deficiency within the smooth muscle and endothelial cell layers was evident in cerebellar white and grey matter arterioles of patients with the m.3243A>G (**B**; Patient 7; COX-succinate dehydrogenase) and the m.8344A>G (**C**; Patient 9, COX-succinate dehydrogenase) mutations. Typically, capillary COX-deficiency was marked relative to dentate neurons where COX activity was intact (**D**; Patient 7, COX-succinate dehydrogenase). Relative to white matter vessels in controls (**E**), mitochondrial density was increased in many vessels of the patients with mitochondrial DNA disease (**F**, Patient 5, Porin immunohistochemistry). Scale bars = 100 μm.

Patient 15; p.Ala467Thr and p.Trp748Ser *POLG* mutations) where ischaemic-lesions were detected (Table 2).

Combined immunohistochemistry and histochemistry using markers of mitochondrial mass, including anti-porin, anti-complex II 70 kDa and succinate dehydrogenase activity, indicated a higher density of mitochondria localized within the vasculature in the majority of patients relative to controls (Fig. 2E and F; Table 2). This was observed in 10/13 patients and included m.3243A>G, m.8344A>G and intriguingly, those patients without evidence of COX-deficiency including those with m.13094T>C and m.14709T>C point mutations, single large-scale mitochondrial DNA deletion and recessive *POLG* mutations.

Morphology of the neurovascular unit

All patients were investigated using immunohistochemical markers for vascular smooth muscle and endothelial cells to evaluate any changes in cellular morphology throughout the cerebellum. Evidence of vascular smooth muscle cell loss was observed with thinning of the vascular smooth muscle cell layer in m.3243A>G (2/3 patients), m.8344A>G (1/1 patient) and m.13094T>C (Fig. 3A). Typically, the vascular smooth muscle cell layer demonstrated a granular, fragmented appearance in the patients with m.3243A>G and m.8344A>G mutations with a decrease in immunoreactivity indicative of vascular smooth muscle cell loss [Fig. 3A(ii and iii)]. Quantitation of alpha-smooth muscle actin immunopositive layer revealed a statistically significant reduction in the thickness of this layer in patients harbouring the m.3243A>G mutation relative to control cases (Fig. 3D; $P < 0.0001$). Evidence of endothelial cell loss was observed with a number of arterioles showing thinning of this layer in patients harbouring m.3243A>G and m.8344A>G [Fig. 3B(i–iii)]. Assessment of the density of astrocytic foot processes surrounding arterioles did not appear to differ between our patients and control cases [Fig. 3C(i–iii)].

High heteroplasmy levels of mutated mitochondrial DNA in the vessel wall

Molecular analysis of the vascular smooth muscle cell and endothelial cell layers of cases with available frozen tissues revealed high percentage levels of mutated mitochondrial DNA in patients with point mutations (Table 3). Typically, patients with the highest (>70%) level of mutated mitochondrial DNA also demonstrated vascular COX-deficiency. These data are in agreement with the segregation of the mutation with the biochemical defect. Skeletal muscle mitochondrial DNA heteroplasmy levels are given as a comparison in Table 3, showing similar levels in skeletal muscle, vascular smooth muscle and endothelial cells.

Immunofluorescent evaluation of the endothelium and tight junction proteins

Immunofluorescent analysis of the endothelium and tight junction proteins was performed on tissues from patients harbouring m.3243A>G ($n = 4$) and m.8344A>G ($n = 1$) relative to age-matched control cases ($n = 4$). Since these cases demonstrated vascular COX-deficiency and morphological changes in the vessel wall, tight junction proteins were assessed as they are known to be affected when the blood–brain barrier is compromised. Evaluation of tight junction morphology and distribution in control cases revealed filamentous immunoreactivity along the vessel endothelium (Fig. 4A–L). In contrast, those patients harbouring the m.3243A>G mutation revealed a redistribution of both ZO-1 and occludin with extrusion of these proteins from the vessel wall into the CNS microenvironment. This was accompanied by obvious thinning and fragmentation of the tight junction proteins (Fig. 4M–X). Evaluation of the tight junction protein expression, ZO-1 and occludin revealed lower fluorescence intensity in m.3243A>G and m.8344A>G relative to control cases (Table 4). This was a significant reduction in fluorescence intensity in m.3243A>G for both ZO-1 and occludin relative to controls ($P < 0.0001$ and $P < 0.0001$, respectively). The lowered fluorescence intensity for ZO-1 and occludin was also observed in m.8344A>G (Table 4 and Fig. 5).

Assessment of the endothelium using GLUT1 showed fragmentation of the endothelial cell layer. Indeed quantitation of immunofluorescent intensity revealed a significant reduction in fluorescence intensity in all m.3243A>G patients assessed relative to control cases ($P < 0.001$, Figs. 4 and 5). Similar levels of GLUT1 fluorescence intensity were detected in a patient harbouring m.8344A>G mutations (Fig. 5 and Table 4). A lowered GLUT1 fluorescence intensity indicates a loss of the endothelium consistent with the immunohistochemistry findings described earlier.

Plasma protein extravasation associated with m.3243A>G and m.8344A>G

Assessment of fibrinogen and IgG in control tissue showed no extravasation of fibrinogen surrounding vessels. However, evidence of Purkinje cell immunoreactivity to fibrinogen and IgG was observed in 4/6 control cases, while the dentate nucleus was spared. In the remaining two cases there was no neuronal immunoreactivity of either Purkinje cells or dentate neurons [Fig. 6A(i and ii)].

The presence of extravascular plasma proteins was observed in all patients demonstrating vascular COX-deficiency and thinning of the endothelial cell layer. Leakage of plasma proteins, including fibrinogen and IgG into the brain microenvironment was observed in patients with m.3243A>G and m.8344A>G mutations. Evaluation of unaffected regions showed weak immunoreactivity for fibrinogen in the neuropil of the white or grey matter depending on the location of the leaky vessel. In general, neurons and glia immunoreactive to fibrinogen and IgG could be detected in the vicinity of the leaky vessels, indicative of neuronal and glial uptake of the plasma proteins. All patients harbouring the m.3243A>G mutation, excluding Patient 3, showed extravasation of fibrinogen, and to a lesser extent IgG; this was accompanied by immunoreactive Purkinje cells indicating neuronal uptake (Table 2). Patient 9 (m.8344A>G mutation) also showed extravasation and Purkinje cell uptake [Fig. 6B(i and ii); Table 4]. Patients with mitochondrial DNA mutations other than m.3243A>G or m.8344A>G demonstrated comparable levels of immunoreactive Purkinje cells to control cases. A number of patients could not be

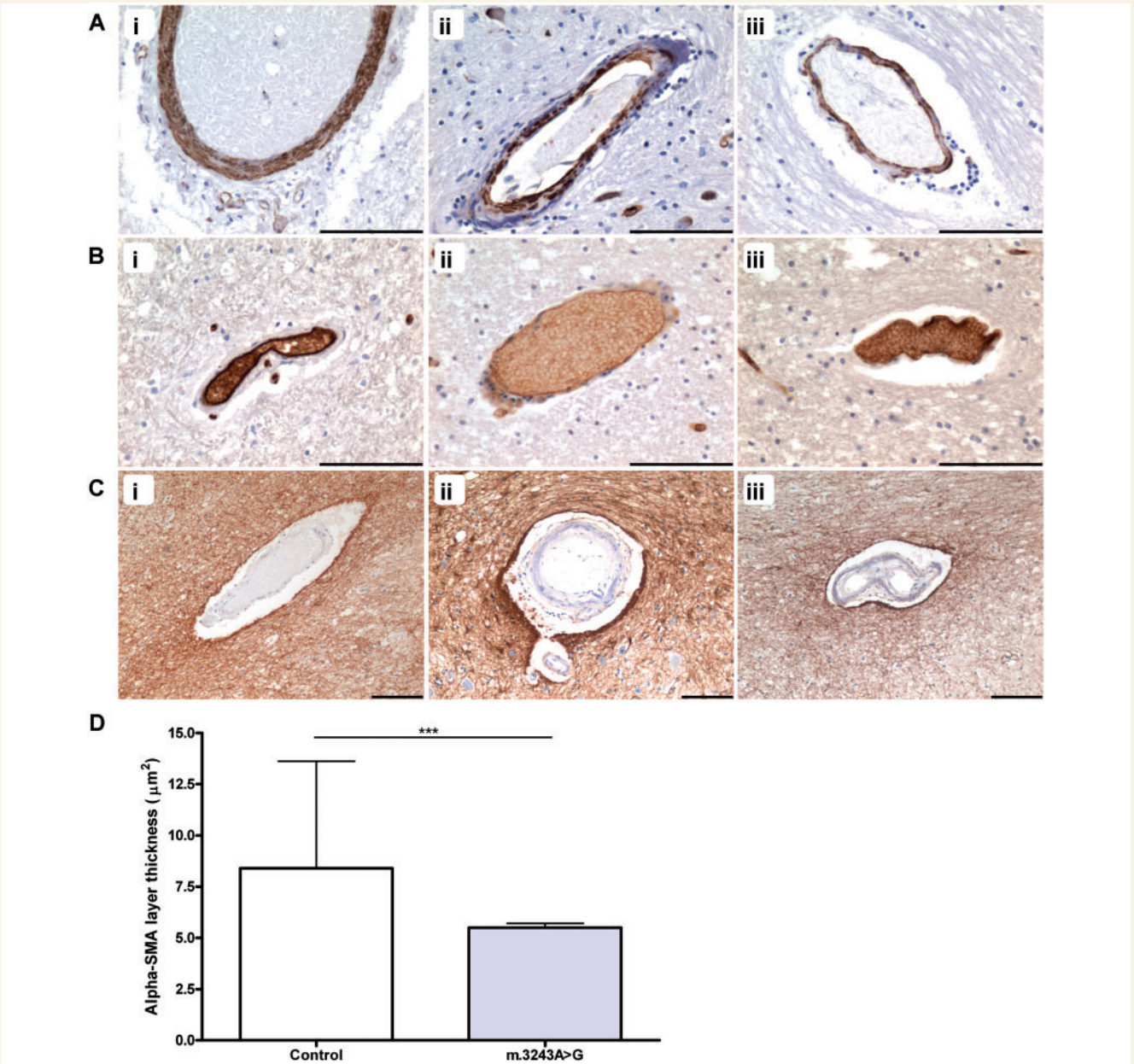

Figure 3 Thinning of vascular smooth muscle and endothelial cell layers in arterioles and high levels of mitochondrial DNA mutation. Relative to vessels in normal controls [**A(i)**]; alpha-smooth muscle actin immunohistochemistry), there is thinning of the vascular smooth muscle cell layer in many patients, particularly those harbouring the m.3243A > G mutation including Patient 1 [**A(ii)**] and Patient 6 [**A(iii)**]. In contrast to control [**B(i)**]; GLUT1 immunohistochemistry), there is also thinning of the endothelial cell layer in numerous patients, including Patient 2 [**B(ii)**] and Patient 7 [**B(iii)**]. Cerebellar vessels in controls [**C(i)**]; glial fibrillary acidic protein immunohistochemistry) and patients (Patient 6, [**C(ii)**]; Patient 7, [**C(iii)**] demonstrate similarly high density of the surrounding astrocytic foot processes. Quantitation of the alpha-smooth muscle actin immunopositive layer shows a significant reduction in thickness in patient arterioles relative to control arterioles (**D**; $***P < 0.0001$). Scale bars = 100 μm.

Table 3 Per cent level mutated mitochondrial DNA in vascular smooth muscle cells, endothelial cells and skeletal muscle

	P1	P2	P3	P4	P5	P6	P7	P8	P9	P10	P11	P12	P13	P14	P15	P16
VSMC (%)	72	ND	ND	84	ND	84	76	80	92	88	51	ND	51	ND	22	28
GLUT1 (%)	71	ND	ND	86	ND	88	87	82	90	86	48	ND	58	42	19	51
Skeletal muscle (%)	72	ND	ND	64	ND	63	72	85	ND	91	83	100	40	ND	ND	ND

ND = not determined; VSMC = vascular smooth muscle cells.

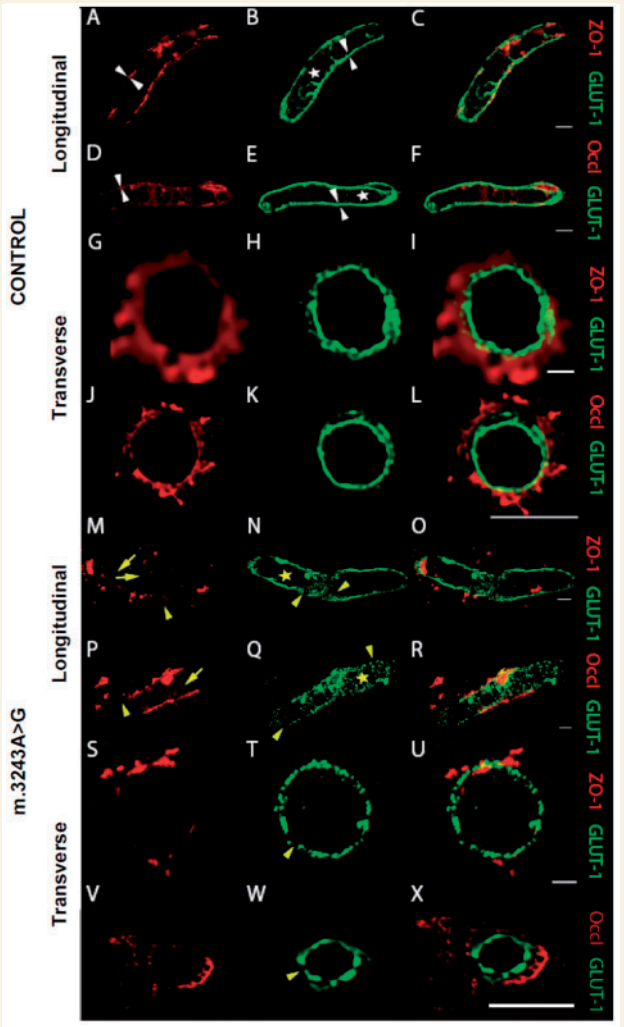

Figure 4 Immunofluorescent images of patient and control cerebellum microvessels, which illustrate the expression and localization of dual-stained endothelium and tight junction proteins. Images from control tissue show the tightly sealed monolayer of the microvascular endothelium, identified by immunofluorescently labeled GLUT1 (**B**, **E**, **H** and **K**; green) and co-stained for tight junction proteins, ZO-1 (**A** and **G**; red) or occludin (**D** and **J**; red). The distribution of ZO-1 and GLUT1 (**C** and **I**) or occludin and GLUT1 (**F** and **L**) can be observed in merged images. BBB pathology is observed in patients harbouring the m.3243A>G mutation. In these patients, there is an absence of an intact GLUT1-positive matrix interna (**N**, **Q**, **T** and **W**; highlighted by yellow star) with evidence of increased fragmentation, decreased immunoreactivity for GLUT1, and increased gap widening between adjacent single endothelial contact points (**N**, **Q** and **T**; yellow arrowheads). In contrast, the control microvessels appear to have an intact and continuous ring of GLUT1-positive endothelial cells within the internal milleau of the microvasculature (**B**, **E**, **H** and **K**; white arrowheads). Disrupted expression of TJ proteins was observed in patients with m.3243A>G compared to controls, including discontinuous staining of ZO-1 (**M**; yellow arrowhead and **S**) and occludin (**P** and **V**; yellow arrowhead). There appears to be increased filtration of these proteins into the brain parenchyma which can be seen on merged images of ZO-1 and GLUT1 (**O** and **U**) or occludin and GLUT1 (**R** and **X**) which was absent in control cases. These pathological signs were consistent with the results obtained from quantifying GLUT1 and TJ protein immunofluorescence, where lower expression levels were demonstrated in patients versus controls. The images were compiled from control and m.3243A>G cerebellum using a x100, oil-based objective and a confocal z-series stack taken every 260 nm throughout the depth of the entire section (6 μm). Images were then deconvolved using Huygens (SVI, v 3.7.1 The Netherlands), with maximum intensity projections rendered in ImageJ. Scale bar = 5–10 μm.

included for analysis due to insufficient tissue sections available for immunostaining.

Extravascular fibrinogen immunoreactivity was also seen diffusely throughout the pan-necrotic lesions of the cerebellar cortex in Patients 4 and 7 (Fig. 6C). In addition to this diffuse expression in the cortex, Purkinje cell and glial cell immunoreactivity was demonstrated suggesting uptake of plasma proteins in these cells [Fig. 6C(i)]. Neighbouring arterioles also showed fibrinogen leakage with intense immunoreactivity in astroglia [Fig. 6C(ii)].

Discussion

Our study confirms that vascular respiratory deficiency occurs in the microvasculature throughout the cerebellum in patients with specific mitochondrial DNA point mutations. While this is particularly prominent in patients harbouring the common m.3243A>G mutation, it is also observed in other patients with other mitochondrial DNA point mutations. In the current study, we have investigated 16 patients to show that vascular respiratory chain deficiency is positively correlated with additional vascular pathology including excess deposition of perivascular collagen and thinning of the vessel wall. We show that there is good correlation between the level of mitochondrial DNA mutation and the development of respiratory chain deficiency. We reveal that the respiratory defect is not limited to vascular smooth muscle cell layer but also involves the endothelial cells, which might be responsible for the structural changes observed in the vessel walls and also breakdown of the blood–brain barrier. From these data, we postulate that microangiopathic changes in the cerebellum occur due to the presence of high levels of mutated mitochondrial DNA and respiratory deficiency within the vessel walls and contribute to the formation of pan-necrotic lesions that play an important role in the genesis of ataxia.

Respiratory chain deficiency in the CNS microvasculature has been reported previously in patients with MELAS and Kearns–Sayre syndrome (Tanji *et al*., 2001; Betts *et al*., 2006). Here, we show that respiratory chain deficiency, as judged by COX/succinate dehydrogenase histochemistry, is most notable in the arterioles supplying the cerebellum of patients harbouring m.3243A>G and m.8344A>G point mutations. In these patients, vascular respiratory deficiency far outweighs any neuronal respiratory deficiency

Table 4 Mean Immunofluorescence intensity values given ± standard deviations for GLUT1, ZO-1 and occludin

Protein	Control cases ($n = 5$)	m.3243A>G ($n = 4$)	m.8344A>G ($n = 1$)
ZO-1	$158.2 \times 10^6 \pm 39.9 \times 10^6$	$100.9 \times 10^6 \pm 23.4 \times 10^6$	$116.2 \times 10^6 \pm 34.7 \times 10^6$
GLUT1	$185.0 \times 10^6 \pm 94.1 \times 10^6$	$75.1 \times 10^6 \pm 31.2 \times 10^6$	$73.0 \times 10^6 \pm 34.7 \times 10^6$
Occludin	$184.4 \times 10^6 \pm 24.1 \times 10^6$	$84.8 \times 10^6 \pm 31.7 \times 10^6$	$105.2 \times 10^6 \pm 62.0 \times 10^6$
GLUT1	$165.2 \times 10^6 \pm 73.4 \times 10^6$	$89.8 \times 10^6 \pm 20.7 \times 10^6$	$61.7 \times 10^6 \pm 42.5 \times 10^6$

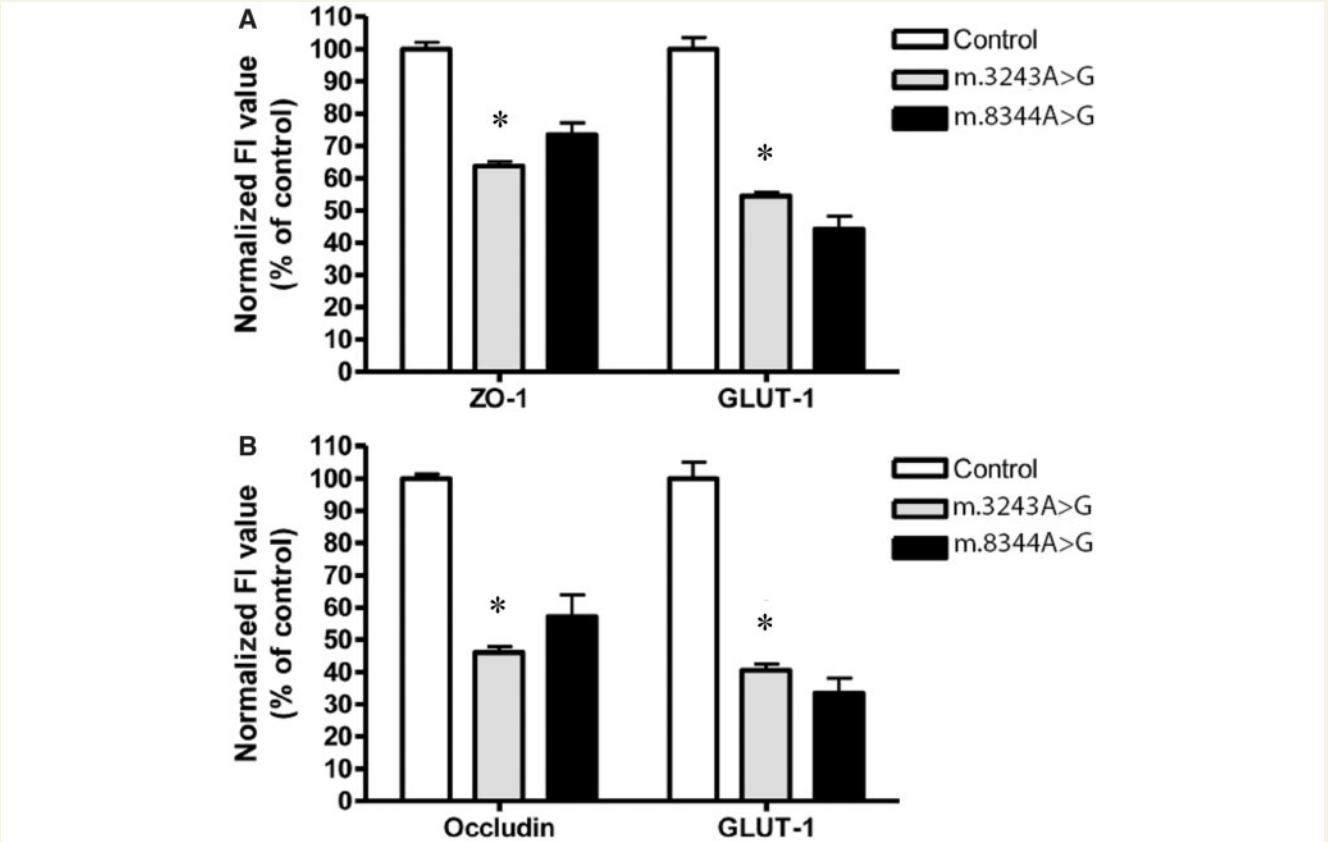

Figure 5 Quantification of the degree of immunoreactivity/expression of tight junction proteins ZO-1 and occludin, and the level of the endothelial marker GLUT1 in the deep white matter of the cerebellum that had been co-expressed with the relevant tight junction protein. Mean fluorescence intensity (FI; in percentage) of ZO-1 co-expressed with GLUT1 in vessels of patients harbouring m.3243A>G and m.8344A>G mutations normalized to control tissue (**A**). Mean fluorescence intensity (in percentage) of occludin co-expressed with GLUT1 in m.3243A>G and m.8344A>G specimens normalized to control tissue (**B**). In each case, the mean control fluorescence intensity was calculated as 100% (mean ± SD). Statistically significant differences between control and m.3243A>G vessels were detected by using the Wilcoxon-Rank Sum Test. Changes in mean fluorescence intensity were detected as highly significant for all proteins examined (*$P < 0.05$).

with most cases demonstrating intact COX-activity in neighbouring neuronal populations.

In addition to respiratory deficiency, we observe increased mitochondrial density in the microvasculature. This has been described before in ultrastructural, histochemical and *in situ* hybridization studies where an aggregation of enlarged mitochondria within the vascular smooth muscle cell and endothelial cell layers are observed (Ohama *et al*., 1987; Sakuta and Nonaka, 1989; Hasegawa *et al*., 1991; Love and Hilton, 1996; Betts *et al*., 2006). Histochemically, these vessels have been termed 'strongly, succinate dehydrogenase-reactive' since they are COX-deficient, but intensely succinate dehydrogenase-reactive. It has been proposed that accumulation of these abnormal mitochondria might lead to occlusion of the vessel and restrict blood flow (Sakuta and Nonaka, 1989). However, we believe it is more likely to be secondary phenomena due to high mutation heteroplasmy levels

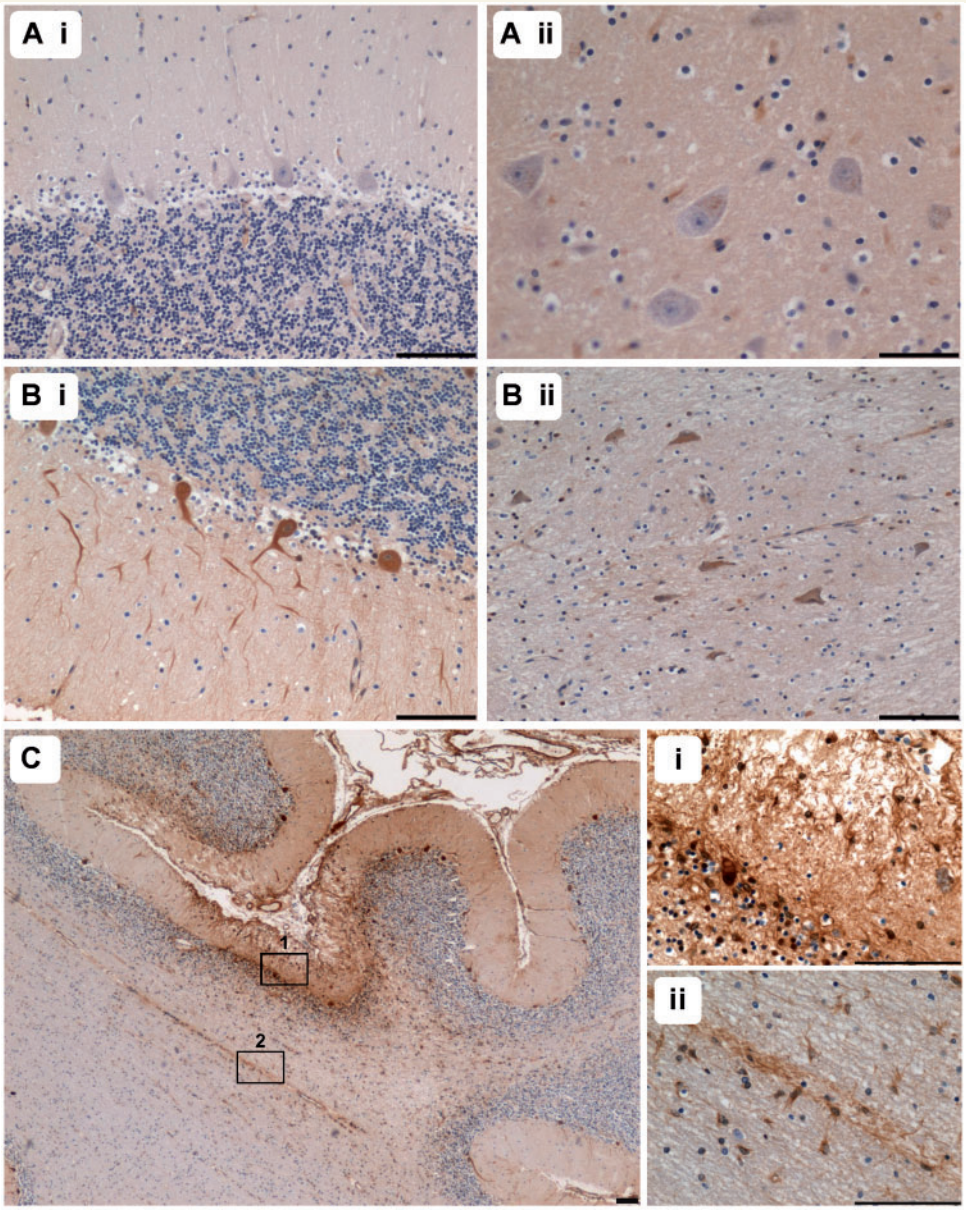

Figure 6 Evidence of blood–brain barrier dysfunction was observed in many patients with extravasation of plasma proteins. Fibrinogen immunohistochemistry in control tissues demonstrated a lack of immunoreactivity in Purkinje cells [**A(i)**] and dentate nucleus neurons [**A(ii)**], while evaluation of a patient with m.8344A > G shows evidence of immunopositive Purkinje cells [**B(i)**], Patient 10) and dentate nucleus neurons [**B(ii)**]. Extravasation of fibrinogen was demonstrated in an ischaemic-like lesion in the cerebellar cortex of Patient 4 (**C**; fibrinogen). Examination at a higher magnification reveals evidence of Purkinje cell uptake [**C(i)**] and immunoreactivity within the molecular and granular cell layers is observed [**C(i)**]. In the adjacent white matter [**C(ii)**], a vessel showing immunoreactivity for fibrinogen is surrounded by immunopositive glial cells. Scale bars = 100 μm.

and therefore reflects a compensatory mechanism whereby mitochondria proliferate, in response to respiratory defects, in order to maintain biochemical activity. This is similar to the ragged red changes frequently observed in skeletal muscle biopsies from these patients.

We observe additional vessel pathology with evidence of arteriole mineralization, which has been described in neuroradiological studies in relation to mitochondrial DNA disease and ageing (Sue *et al*., 1998; Ostling *et al*., 2003). The precise mechanisms of mineralization are not well understood; however, it has been postulated that vascular smooth muscle cell dysfunction is the main driving force for mineralization (Speer *et al*., 2009). This is a particularly intriguing suggestion since we observe high levels of mitochondrial DNA mutations and respiratory deficiency in the vascular smooth muscle cell layer and immunohistochemical evidence of a loss of vascular smooth muscle cells from the arteriole wall. The

vascular smooth muscle cells are crucial in the control and maintenance of vascular tone and therefore regulate blood flow. If these cells are energetically compromised, this could perturb vascular tone and impede the ability of the vascular smooth muscle cells to adapt to alteration in the microenvironment, also known as functional hyperaemia. Further evidence in support of impaired vascular tone may derive from our observed increase in collagen IV immunoreactivity in the microvasculature indicating an increase in the thickness of the basement membrane and hyalinosis, which might be related to endothelial cell and vascular smooth muscle cell dysfunction.

Marked reduction in endothelial cell thickness and fragmentation of this cell layer is seen in patients exhibiting vascular COX-deficiency. The CNS endothelium plays an essential role in maintaining integrity of the blood–brain barrier and preventing harmful substances from reaching neuronal cells (Bradbury, 1993). It achieves this by way of a continuous ring of tight junction proteins that are situated between adjacent endothelial cells. Here, we show a loss of two key tight junction proteins, ZO-1 and occludin, in those patients demonstrating high levels of m.3243A>G and m.8344A>G mitochondrial DNA mutations, COX-deficiency and abnormal vessel morphology. Growing evidence suggests that an impairment of the blood–brain barrier correlates with a decrease of tight junctions in the endothelial layer (Clatterbuck *et al*., 2001; Glading *et al*., 2007). In conjunction with this, there is extrusion of plasma proteins into the brain parenchyma providing further evidence of compromised blood–brain barrier associated with m.3243A>G and m.8344A>G mutations in agreement with earlier findings in a patient with MELAS (Tanji *et al*., 2001). A recent *in vitro* blood–brain barrier model consisting of CNS astrocytes and endothelial cells has shown that in the presence of high levels of the m.3243A>G mutation, the blood–brain barrier becomes compromised. They showed that the endothelial cells demonstrate COX-deficiency and also have markedly lowered trans-endothelial electrical resistance suggesting an increase in blood–brain barrier permeability (Davidson *et al*., 2009). The contribution of blood–brain barrier dysfunction due to mitochondrial DNA defects to neurodegeneration remains to be elucidated; however, extravasation of plasma proteins might present an extra burden on neural function. This is an important area of investigation since blood–brain barrier dysfunction has been documented in other mitochondrial DNA disorders, including mitochondrial neurogastrointestinal encephalopathy (MNGIE) (Szigeti *et al*., 2004).

Our study shows that pan-necrotic lesions are common in the cerebellum of patients with mitochondrial DNA point mutations (m.3243A>G and m.8344A>G) and nuclear mutations in *POLG* causing secondary defects of the mitochondrial DNA. In association with this, there is evidence of vascular COX-deficiency involving all arterioles and changes in the density of vascular smooth muscle cell and endothelial cells. How these deficiencies contribute to the focal vascular events is uncertain. We certainly do not detect any evidence of occlusion and in our view the vascular smooth muscle deficiency is likely to lead to impaired regulation of blood supply and local ischaemia due to an absent response to localized changes in energy demand. This is a feasible hypothesis since smooth muscle dysfunction in the bowel wall of patients with m.3243A>G is thought to be the cause of bowel dysmotility in these patients (Betts *et al*., 2008). In addition to the vascular smooth muscle cell pathology, respiratory deficiency observed in endothelial cells might affect the formation of tight junction and therefore impair cell–cell contacts resulting in blood–brain barrier breakdown. Blood–brain barrier disruption might present an additional strain on neighbouring neurons and glial cells since they appear to actively uptake plasma protein components to remove them from the brain microenvironment (Matz *et al*., 2001). It has been suggested that uptake by neurons and astrocytes may merely represent post-mortem changes in blood–brain barrier permeability (Mori *et al*., 1991; Munoz *et al*., 1997); however, plasma protein extravasation was much higher in patient tissues compared to control indicating that changes in localization of fibrinogen and IgG are true pathological alterations. In fact, a recent study links fibrinogen leakage into the brain parenchyma with neuronal damage in Alzheimer's disease (Cortes-Canteli *et al*., 2010).

This study expands on the complicated story of neurodegeneration in mitochondrial DNA disease where multiple mechanisms likely exist to contribute to dysfunction and degeneration of the CNS. Critically, this study shows respiratory deficiency in vessels from patients with other mitochondrial DNA mutations, not just m.3243A>G and the extent to which the microvasculature is pathologically affected. This area of neurodegeneration is important since the microvasculature might present a feasible target for therapeutic intervention and thus modulation of disease progression.

Acknowledgements

Tissue for this study was provided by the Newcastle Brain Tissue Resource, which is funded in part by a grant from the UK Medical Research Council (G0400074). The authors wish to express their gratitude to Dr. Joanna Elson for her statistical support when interpreting the immunofluorescent work performed during this study. Authors also wish to thank Dr. Glyn Nelson for his expert advice rendered in the design of the protocol for analysing the tight junction and GLUT1 immunofluorescence.

Funding

The Wellcome Trust Centre for Mitochondrial Research (906919), the Newcastle University Centre for Brain Ageing and Vitality supported by BBSRC, EPSRC, ESRC and MRC as part of the cross-council Lifelong Health and Wellbeing Initiative (G0700718), UK NIHR Biomedical Research Centre for Ageing and Age-related disease award to the Newcastle upon Tyne Hospitals NHS Foundation Trust and the UK NHS Specialist Commissioners, which funds the 'Rare Mitochondrial Disorders of Adults and Children' Diagnostic Service in Newcastle upon Tyne (http://www.mitochondrialncg.nhs.uk), Medical Research Council, Biotechnology and Biosciences Research Council, Engineering and Physical Sciences Research Council, Economic and Social Research Council.

Supplementary material

Supplementary material is available at *Brain* online.

References

Alston CL, Lowe J, Turnbull DM, Maddison P, Taylor RW. A novel mitochondrial tRNAGlu (MTTE) gene mutation causing chronic progressive external ophthalmoplegia at low levels of heteroplasmy in muscle. J Neurol Sci 2010; 298: 140–4.

Bender A, Krishnan KJ, Morris CM, Taylor GA, Reeve AK, Perry RH, et al. High levels of mitochondrial DNA deletions in substantia nigra neurons in aging and Parkinson disease. Nat Genet 2006; 38: 515–17.

Betts J, Barron MJ, Needham SJ, Schaefer AM, Taylor RW, Turnbull DM. Gastrointestinal tract involvement associated with the 3243A>G mitochondrial DNA mutation. Neurology 2008; 70: 1290–2.

Betts J, Jaros E, Perry RH, Schaefer AM, Taylor RW, Abdel-All Z, et al. Molecular neuropathology of MELAS: level of heteroplasmy in individual neurones and evidence of extensive vascular involvement. Neuropathol Appl Neurobiol 2006; 32: 359–73.

Betts-Henderson J, Jaros E, Krishnan KJ, Perry RH, Reeve AK, Schaefer AM, et al. Alpha-synuclein pathology and Parkinsonism associated with POLG1 mutations and multiple mitochondrial DNA deletions. Neuropathol Appl Neurobiol 2009; 35: 120–4.

Bradbury MW. The blood-brain barrier. Exp Physiol 1993; 78: 453–72.

Clatterbuck RE, Eberhart CG, Crain BJ, Rigamonti D. Ultrastructural and immunocytochemical evidence that an incompetent blood–brain barrier is related to the pathophysiology of cavernous malformations. J Neurol Neurosurg Psychiatry 2001; 71: 188–92.

Cortes-Canteli M, Paul J, Norris EH, Bronstein R, Ahn HJ, Zamolodchikov D, et al. Fibrinogen and beta-amyloid association alters thrombosis and fibrinolysis: a possible contributing factor to Alzheimer's disease. Neuron 2010; 66: 695–709.

Davidson MM, Walker WF, Hernandez-Rosa E. The m.3243A>G mtDNA mutation is pathogenic in an in vitro model of the human blood brain barrier. Mitochondrion 2009; 9: 463–70.

Deschauer M, Tennant S, Rokicka A, He L, Kraya T, Turnbull DM, et al. MELAS associated with mutations in the POLG1 gene. Neurology 2007; 68: 1741–2.

DiMauro S, Schon EA. Mitochondrial disorders in the nervous system. Annu Rev Neurosci 2008; 31: 91–123.

Fuseler JW, Bedenbaugh A, Yekkala K, Baudino TA. Fractal and image analysis of the microvasculature in normal intestinal submucosa and intestinal polyps in Apc(Min/+) mice. Microsc Microanal 2010; 16: 73–9.

Fuseler JW, Merrill DM, Rogers JA, Grisham MB, Wolf RE. Analysis and quantitation of NF-kappaB nuclear translocation in tumor necrosis factor alpha (TNF-α) activated vascular endothelial cells. Microsc Microanal 2006; 12: 269–76.

Gilchrist JM, Sikirica M, Stopa E, Shanske S. Adult-onset MELAS. Evidence for involvement of neurons as well as cerebral vasculature in strokelike episodes. Stroke 1996; 27: 1420–3.

Glading A, Han J, Stockton RA, Ginsberg MH. KRIT-1/CCM1 is a Rap1 effector that regulates endothelial cell cell junctions. J Cell Biol 2007; 179: 247–54.

Guan Y, Watson AJ, Marchiando AM, Bradford E, Shen L, Turner JR, et al. Redistribution of the tight junction protein ZO-1 during physiological shedding of mouse intestinal epithelial cells. Am J Physiol Cell Physiol 2011; 300: C1404–14.

Hasegawa H, Matsuoka T, Goto Y, Nonaka I. Strongly succinate dehydrogenase-reactive blood vessels in muscles from patients with mitochondrial myopathy, encephalopathy, lactic acidosis, and stroke-like episodes. Ann Neurol 1991; 29: 601–5.

Iizuka T, Sakai F. Pathogenesis of stroke-like episodes in MELAS: analysis of neurovascular cellular mechanisms. Curr Neurovasc Res 2005; 2: 29–45.

Iizuka T, Sakai F, Ide T, Miyakawa S, Sato M, Yoshii S. Regional cerebral blood flow and cerebrovascular reactivity during chronic stage of stroke-like episodes in MELAS—implication of neurovascular cellular mechanism. J Neurol Sci 2007; 257: 126–38.

Iizuka T, Sakai F, Kan S, Suzuki N. Slowly progressive spread of the stroke-like lesions in MELAS. Neurology 2003; 61: 1238–44.

Iizuka T, Sakai F, Suzuki N, Hata T, Tsukahara S, Fukuda M, et al. Neuronal hyperexcitability in stroke-like episodes of MELAS syndrome. Neurology 2002; 59: 816–24.

Koga Y, Akita Y, Nishioka J, Yatsuga S, Povalko N, Tanabe Y, et al. L-Arginine improves the symptoms of strokelike episodes in MELAS. Neurology 2005; 64: 710–12.

Koga Y, Povalko N, Nishioka J, Katayama K, Kakimoto N, Matsuishi T. MELAS and L-arginine therapy: pathophysiology of stroke-like episodes. Ann NY Acad Sci 2010; 1201: 104–10.

Krishnan KJ, Bender A, Taylor RW, Turnbull DM. A multiplex real-time PCR method to detect and quantify mitochondrial DNA deletions in individual cells. Anal Biochem 2007; 370: 127–9.

Lax NZ, Hepplewhite PD, Reeve AK, Nesbitt V, McFarland R, Jaros E, et al. Cerebellar ataxia in patients with mitochondrial DNA disease: a molecular clinico-pathological study. J Neuropathol Exp Neurol 2012a; 71: 148–61.

Lax NZ, Whittaker RG, Hepplewhite PD, Reeve AK, Blakely E, Jaros E, et al. Sensory neuronopathy in patients harbouring recessive polymerase gamma mutations. Brain 2012b; 135: 62–71.

Love S, Hilton DA. Assessment of the distribution of mitochondrial ribosomal RNA in melas and in thrombotic cerebral infarcts by in situ hybridization. J Pathol 1996; 178: 182–9.

Matz PG, Lewen A, Chan PH. Neuronal, but not microglial, accumulation of extravasated serum proteins after intracerebral hemolysate exposure is accompanied by cytochrome c release and DNA fragmentation. J Cereb Blood Flow Metab 2001; 21: 921–8.

Mori S, Sternberger NH, Herman MM, Sternberger LA. Leakage and neuronal uptake of serum protein in aged and Alzheimer brains. A postmortem phenomenon with antemortem etiology. Lab Invest 1991; 64: 345–51.

Munoz DG, Erkinjuntti T, Gaytan-Garcia S, Hachinski V. Serum protein leakage in Alzheimer's disease revisited. Ann NY Acad Sci 1997; 826: 173–89.

Ohama E, Ohara S, Ikuta F, Tanaka K, Nishizawa M, Miyatake T. Mitochondrial angiopathy in cerebral blood vessels of mitochondrial encephalomyopathy. Acta Neuropathol 1987; 74: 226–33.

Ohama E, Ohara S, Ikuta F, Tanaka K, Nishizawa M, Miyatake T. [Mitochondrial angiopathy in the cerebral blood vessels of MELAS (mitochondrial myopathy, encephalopathy, lactic acidosis and stroke-like episodes)]. No To Shinkei 1988; 40: 109–18.

Ostling S, Andreasson LA, Skoog I. Basal ganglia calcification and psychotic symptoms in the very old. Int J Geriatr Psychiatry 2003; 18: 983–7.

Pavlakis SG, Phillips PC, DiMauro S, De Vivo DC, Rowland LP. Mitochondrial myopathy, encephalopathy, lactic acidosis, and stroke-like episodes: a distinctive clinical syndrome. Annals of Neurology 1984; 16: 481–8.

Sakuta R, Nonaka I. Vascular involvement in mitochondrial myopathy. Ann Neurol 1989; 25: 594–601.

Sparaco M, Bonilla E, DiMauro S, Powers JM. Neuropathology of mitochondrial encephalomyopathies due to mitochondrial DNA defects. J Neuropathol Exp Neurol 1993; 52: 1–10.

Speer MY, Yang HY, Brabb T, Leaf E, Look A, Lin WL, et al. Smooth muscle cells give rise to osteochondrogenic precursors and chondrocytes in calcifying arteries. Circ Res 2009; 104: 733–41.

Sue CM, Crimmins DS, Soo YS, Pamphlett R, Presgrave CM, Kotsimbos N, et al. Neuroradiological features of six kindreds with MELAS tRNA(Leu) A2343G point mutation: implications for pathogenesis. J Neurol Neurosurg Psychiatry 1998; 65: 233–40.

Szigeti K, Sule N, Adesina AM, Armstrong DL, Saifi GM, Bonilla E, et al. Increased blood-brain barrier permeability with thymidine phosphorylase deficiency. Ann Neurol 2004; 56: 881–6.

Tanji K, DiMauro S, Bonilla E. Disconnection of cerebellar Purkinje cells in Kearns-Sayre syndrome. J Neurol Sci 1999a; 166: 64–70.

Tanji K, Gamez J, Cervera C, Mearin F, Ortega A, de la Torre J, et al. The A8344G mutation in mitochondrial DNA associated with stroke-like episodes and gastrointestinal dysfunction. Acta Neuropathol 2003; 105: 69–75.

Tanji K, Kunimatsu T, Vu TH, Bonilla E. Neuropathological features of mitochondrial disorders. Semin Cell Dev Biol 2001; 12: 429–39.

Tanji K, Vu TH, Schon EA, DiMauro S, Bonilla E. Kearns-Sayre syndrome: unusual pattern of expression of subunits of the respiratory chain in the cerebellar system. Ann Neurol 1999b; 45: 377–83.

Taylor RW, Barron MJ, Borthwick GM, Gospel A, Chinnery PF, Samuels DC, et al. Mitochondrial DNA mutations in human colonic crypt stem cells. J Clin Invest 2003; 112: 1351–60.

Tokunaga M, Mita S, Sakuta R, Nonaka I, Araki S. Increased mitochondrial DNA in blood vessels and ragged-red fibers in mitochondrial myopathy, encephalopathy, lactic acidosis, and stroke-like episodes (MELAS). Ann Neurol 1993; 33: 275–80.

Tuppen HA, Blakely EL, Turnbull DM, Taylor RW. Mitochondrial DNA mutations and human disease. Biochim Biophys Acta 2010; 1797: 113–28.

Tzoulis C, Engelsen BA, Telstad W, Aasly J, Zeviani M, Winterthun S, et al. The spectrum of clinical disease caused by the A467T and W748S POLG mutations: a study of 26 cases. Brain 2006; 129: 1685–92.

Tzoulis C, Neckelmann G, Mork SJ, Engelsen BE, Viscomi C, Moen G, et al. Localized cerebral energy failure in DNA polymerase gamma-associated encephalopathy syndromes. Brain 2010; 133: 1428–37.

Winterthun S, Ferrari G, He L, Taylor RW, Zeviani M, Turnbull DM, et al. Autosomal recessive mitochondrial ataxic syndrome due to mitochondrial polymerase gamma mutations. Neurology 2005; 64: 1204–8.

Yamamoto Y, Ihara M, Tham C, Low RW, Slade JY, Moss T, et al. Neuropathological correlates of temporal pole white matter hyperintensities in CADASIL. Stroke 2009; 40: 2004–11.